Circulation: Arrhythmia and Electrophysiology

ORIGINAL ARTICLE

Electrophysiology and Arrhythmogenesis in the Human Right Ventricular Outflow Tract

Kedar Aras, PhD; Anna Gams, BS; Ndeye Rokhaya Faye, PhD; Jaclyn Brennan, PhD; Katherine Goldrick, BS; Jinghua Li, PhD; Yishan Zhong, PhD; Chia-Han Chiang, PhD; Elizabeth H. Smith, BS; Megan D. Poston, BS; Jacqueline Chivers, BS; Peter Hanna, MD, PhD; Shumpei Mori, MD, PhD; Olujimi A. Ajijola, MD, PhD; Kalyanam Shivkumar, MD, PhD; Donald B. Hoover, PhD; Jonathan Viventi, PhD; John A. Rogers, PhD; Olivier Bernus, PhD; Igor R. Efimov, PhD

BACKGROUND: Right ventricular outflow tract (RVOT) is a common source of ventricular tachycardia, which often requires ablation. However, the mechanisms underlying the RVOT's unique arrhythmia susceptibility remain poorly understood due to lack of detailed electrophysiological and molecular studies of the human RVOT.

METHODS: We conducted optical mapping studies in 16 nondiseased donor human RVOT preparations subjected to pharmacologically induced adrenergic and cholinergic stimulation to evaluate susceptibility to arrhythmias and characterize arrhythmia dynamics.

RESULTS: We found that under control conditions, RVOT has shorter action potential duration at 80% repolarization relative to the right ventricular apical region. Treatment with isoproterenol (100 nM) shortened action potential duration at 80% repolarization and increased incidence of premature ventricular contractions (P=0.003), whereas acetylcholine (100 μM) stimulation alone had no effect on action potential duration at 80% repolarization or premature ventricular contractions. However, acetylcholine treatment after isoproterenol stimulation reduced the incidence of premature ventricular contractions (P=0.034) and partially reversed action potential duration at 80% repolarization shortening (P=0.029). Immunolabeling of RVOT (n=4) confirmed the presence of cholinergic marker VAChT (vesicular acetylcholine transporter) in the region. Rapid pacing revealed RVOT susceptibility to both concordant and discordant alternans. Investigation into transmural arrhythmia dynamics showed that arrhythmia wave fronts and phase singularities (rotors) were relatively more organized in the endocardium than in the epicardium (P=0.006). Moreover, there was a weak but positive spatiotemporal autocorrelation between epicardial and endocardial arrhythmic wave fronts and rotors. Transcriptome analysis (n=10 hearts) suggests a trend that MAPK (mitogen-activated protein kinase) signaling, calcium signaling, and cGMP-PKG (protein kinase G) signaling are among the pathways that may be enriched in the male RVOT, whereas pathways of neurodegeneration may be enriched in the female RVOT.

CONCLUSIONS: Human RVOT electrophysiology is characterized by shorter action potential duration relative to the right ventricular apical region. Cholinergic right ventricular stimulation attenuates the arrhythmogenic effects of adrenergic stimulation, including increase in frequency of premature ventricular contractions and shortening of wavelength. Right ventricular arrhythmia is characterized by positive spatial-temporal autocorrelation between epicardial-endocardial arrhythmic wave fronts and rotors that are relatively more organized in the endocardium.

GRAPHIC ABSTRACT: A graphic abstract is available for this article.

Key Words: acetylcholine ■ arrhythmias, cardiac ■ heart ventricles ■ isoproterenol ■ ventricular premature complexes

Correspondence to: Igor R. Efimov, PhD, Department of Biomedical Engineering, George Washington University, Science and Engineering Hall, 800 22nd Street NW, Washington, DC, 20052, Email efimov@gwu.edu or Kedar Aras, PhD, Department of Biomedical Engineering, George Washington University, Science and Engineering Hall, 800 22nd Street NW, Washington, DC, 20052, Email kedar_aras@gwu.edu

Supplemental Material is available at https://www.ahajournals.org/doi/suppl/10.1161/CIRCEP.121.010630.
For Sources of Funding and Disclosures, see page 180.

Circulation: Arrhythmia and Electrophysiology is available at www.ahajournals.org/journal/circep

WHAT IS KNOWN?

- Right ventricular outflow tract is a common source of idiopathic ventricular arrhythmias.
- However, the mechanisms underlying the right ventricular outflow tract's unique arrhythmia susceptibility remain not well elucidated due to lack of detailed electrophysiological and molecular studies of human right ventricular outflow tract.

WHAT THE STUDY ADDS

- Human right ventricular outflow tract electrophysiology is characterized by shorter action potential duration relative to the right ventricular apical region and drives the transmural dispersion of repolarization and transmural action potential duration dispersion under normal physiological conditions.
- Cholinergic stimulation attenuates the arrhythmogenic effects of adrenergic stimulation, including increase in frequency of premature ventricular contractions and shortening of wavelength.
- Arrhythmia in the right ventricle is associated with weak positive spatiotemporal autocorrelation between the epicardial-endocardial arrhythmic wave fronts and reentrant rotors that are relatively more organized in the endocardium.

Nonstandard Abbreviations and Acronyms

APD	action potential duration
APD80	action potential duration at 80% repolarization
DF	dominant frequency
MAPK	mitogen-activated protein kinase
MMVT	monomorphic ventricular tachycardia
PGP9.5	protein gene product 9.5
PKG	protein kinase G
PS	phase singularity
PVC	premature ventricular contraction
RV	right ventricle
RVAR	right ventricular apical region
RVOT	right ventricular outflow tract
S1S1	basic pulse pacing protocol
Th	tyrosine hydroxylase
VAChT	vesicular acetylcholine transporter
VF	ventricular fibrillation
VT	ventricular tachycardia

The right ventricular outflow tract (RVOT) is a dominant site of origin of premature ventricular contractions (PVCs) and ventricular tachyarrhythmias including the Brugada syndrome, idiopathic ventricular arrhythmias, and arrhythmogenic right ventricular (RV) cardiomyopathy among others.[1,2] Anatomically, the RVOT is a thin, smooth-walled, tubular structure located between the pulmonary artery and inlet and apical components of the RV. The tissue structure is interspersed with heterogenous distribution of fibrous and fat tissue[3,4] and comprises a complex 3-dimensional network of cardiac fibers arranged circumferentially in the subepicardium and longitudinally in the sub-endocardium.[5] Moreover, the RVOT–pulmonary root junction is characterized by multiple tissue types including the myocardium, valve, and smooth muscle tissue, with the myocardium of the free-standing subpulmonary infundibulum commonly supporting the bases of the three pulmonary sinuses.[6] Given the complex anatomic makeup and the presence of endocardial Purkinje network,[7] the RVOT could be predisposed to arrhythmogenesis, as suggested by the observation that ≈80% of idiopathic ventricular arrhythmias originate in the RVOT.[8] While there have been basic RVOT studies in mice,[9,10] rabbit,[11,12] porcine,[13] and canine[14,15] animal models, the electrophysiological and arrhythmogenic profile of healthy human RVOT remains poorly studied.

The autonomic nervous system plays an important regulatory role in cardiac physiology, and the dysfunction of the autonomic nervous system associated with sympathovagal imbalances has been linked to cardiac arrhythmias.[16,17] While sympathetic modulation affects both the atria and the ventricles, the current paradigm suggests that the parasympathetic control is limited to the atria and that direct parasympathetic modulation of the ventricles is insignificant.[18] Evidence suggests the presence of cholinergic innervation in the ventricles in various species,[19,20] but the functional significance of direct parasympathetic influence on ventricles is not well-established or characterized.

Both focal and reentrant mechanisms play a role in arrhythmogenesis, with reentry believed to be the primary mechanism of maintenance of sustained ventricular arrhythmias[21] and focal sources serving as triggers. However, controversy remains on the mechanism of reentrant arrhythmia: is it driven by multiple wavelets or a single mother rotor?[22] Recent studies have also suggested that endocardial and epicardial dissociation may play a role in the maintenance of atrial arrhythmias.[23] However, the role of endocardial-epicardial dissociation in the maintenance of ventricular arrhythmias is not well-characterized.

In this study, we aimed to fill the existing knowledge gap in characterization of human RVOT electrophysiology using dual-sided (epicardial and endocardial) optical and electrical mapping of the RV from donor human hearts and to characterize transcriptome and protein expression in combination with RNA sequencing and immunohistochemistry, respectively. Using these techniques, we provide novel functional, structural, and transcriptomic profile of nonpathological human RVOT.

MATERIALS AND METHODS

The data, methods, and study materials will be made available for other researchers upon request for the purposes of developing new methods of analysis, reproducing the results, or replicating the procedure. Detailed description of the materials and methods is available in the Supplemental Material.

Study Design

All studies (n=30) using deidentified human heart tissue were approved by the Institutional Review Board at the George Washington University and University of California, Los Angeles. In total for this study, we procured 29 deidentified donor human hearts from the Washington Regional Transplant Community. One additional donor heart was procured through the University of California at Los Angeles Cardiac Arrhythmia Center in Los Angeles, California. All hearts were arrested using ice-cold cardioplegic solution in the operating room and transported to the laboratory for dissection and subsequent electrophysiology, transcriptome, and immunostaining studies. A complete list of hearts with available clinical information is shown in Figure S1.

This was a prospective, nonrandomized study, and the investigators were not blinded to the data. Three donor hearts (group 0) were used to conduct exploratory research including development of study protocol and the techniques for RVOT wedge dissection, cannulation, and perfusion. Donor hearts were grouped to investigate the effects of cholinergic and adrenergic modulation using optical mapping. Group 1 (n=7; male, 3; female, 4) donor hearts were used to study the effects of cholinergic and adrenergic stimulation in isolation. Group 2 (n=6; male, 3; female, 3) was used to evaluate the effects of cholinergic stimulation in donor hearts already subjected to adrenergic stimulation. Since fresh tissue samples could not be extracted from groups 1 and 2, additional group 3 donor hearts were used to collect tissue for RNA sequencing (n=10; male, 5; female, 5) and immunostaining (n=4; male, 1; female, 3) studies. Group 3 was not subjected to functional studies to avoid likely changes in transcriptome caused by in vitro perfusion. While optical mapping was the primary modality for functional studies, we also conducted simultaneous optical and electrical mapping in 3 donor hearts to validate optical mapping with a clinically relevant electrical mapping.

All data and software used for functional, transcriptomic, and immunostaining studies will be made available through the online repository at the George Washington University.

Experimental Preparation and Study Protocol

Dual-sided (epicardial and endocardial) optical and electrical mapping experiments were conducted in RVOT preparations from donor human hearts (Figure 1A). To prepare the RVOT wedge preparation, the aorta and the pulmonary artery were dissected open to expose and isolate the right and left coronary arteries for cannulation. Most of the atria, the left ventricle, and the posterior RV were removed to expose the anterior RV and the RVOT surface area. The remaining vessel branches were tied off. The RVOT preparation was stretched across a frame and secured to pull it flat (Figure 1B). The tissue was suspended vertically in a bath to allow optical access to both the endocardial and epicardial surface and immobilized by blebbistatin (10–15 μM) to suppress motion artifacts in optical recordings, without adverse electrophysiological effects.[24] Di-4-ANBDQBS was used to map transmembrane potential as described previously.[25]

Tissue was paced from the endocardium using a dynamic restitution protocol (basic pulse pacing protocol [S1S1]) to assess rate dependence of action potential duration (APD). Briefly, the S1S1 protocol entails pacing the tissue for at least 60 beats at constant cycle length (S1S1) and then repeating the process by progressively shortening the S1-S1 intervals. This restitution protocol was executed after each treatment. For group 1, the tissue was treated with acetylcholine (100 μM) and the restitution protocol repeated. Following that, acetylcholine was washed out, and the tissue was treated with isoproterenol (100 nmol/L). The restitution protocol was repeated until arrhythmia was induced (Figure 1C). For group 2, the tissue was first treated with isoproterenol (100 nmol/L) and the restitution protocol repeated. The tissue was then subjected to acetylcholine (100 μM) treatment, while still under the influence of sympathetic stimulation (no washout of isoproterenol). In case the S1S1 restitution protocol alone was unable to induce arrhythmia, burst pacing (50 Hz) in combination with pinacidil (50 μM) was used for arrhythmia induction. Only in 2 cases (D3 and D10), we were unable to induce arrhythmia. All arrhythmia inductions were sustained and lasted for at least 15 minutes. We chose an aggressive arrhythmia induction protocol as ventricular tachycardia (VT) is only occasionally initiated by PVCs originating from the RVOT.[26]

OPTICAL CARDIAC MAPPING

Optical action potentials were mapped from ≈7×7 cm field of view from the two surfaces (epicardium and endocardium) using 2 MiCAM05 (SciMedia, CA) CMOS cameras (100×100 pixels). All optical signals were processed in MATLAB-based custom open-source software RHYTHM. Activation times were determined by calculating the time of dF/dt_{max}, which corresponds to the steepest segment of the optical action potential upstroke (Figure S2A). APD was calculated at 80% repolarization (APD80). To measure the extent of spatial organization during ventricular tachyarrhythmia, indices including dominant frequency (DF), regularity index, and organization index were evaluated for each pixel.[27] To evaluate the complexity of arrhythmias including wave front dynamics, phase singularity (PS) dynamics, and endocardial-epicardial dissociation dynamics, the optical signals were transformed into the phase domain using the Hilbert transform (Figure S2B).

Wave fronts were defined as the isophase lines along $\phi=\varpi/2$.[28] The number of discrete wave fronts was calculated for each field of view and tracked over its life span. Wave fronts smaller than 20 pixels (≈14 mm) were treated as noise and not included in the analysis. Wave

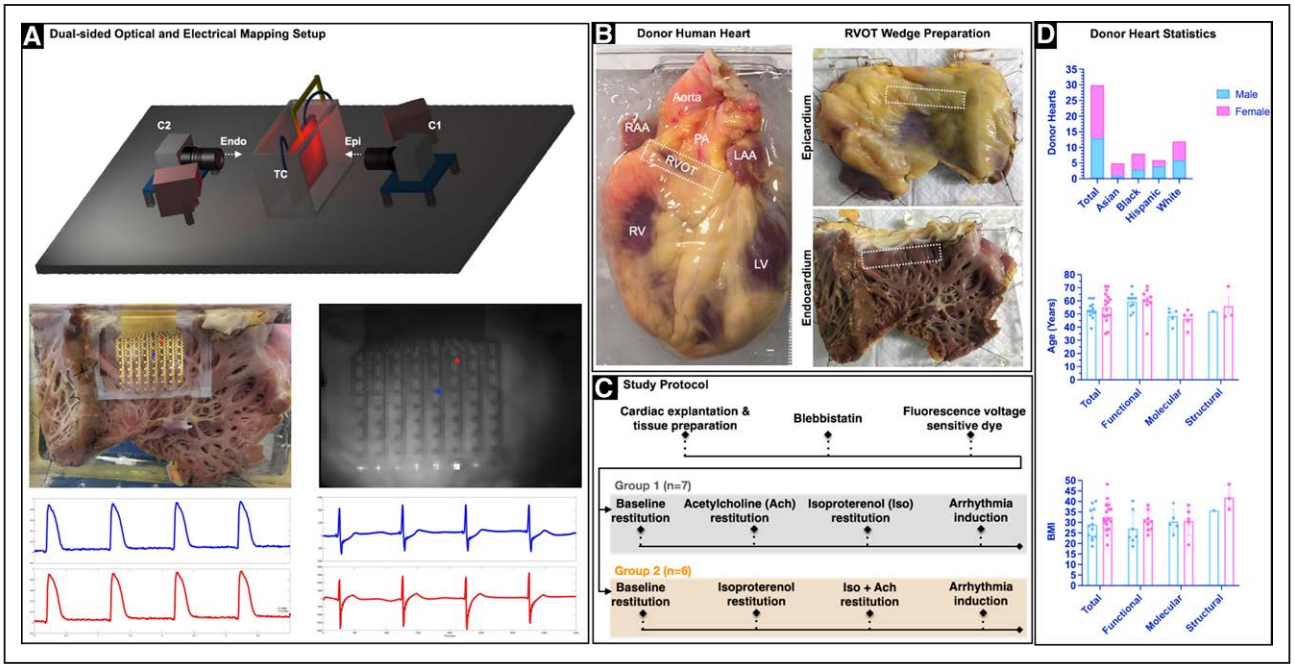

Figure 1. Experimental setup and study protocol.

A, Schematic of the dual-sided optical mapping setup (**top**). A 64-electrode passive stretchable and translucent array to record electrical signals simultaneously with optical signals. Representative sample optical action potentials and electrograms from 2 locations on the endocardial surface are shown (**bottom**). **B**, Representative donor human heart and right ventricular outflow tract (RVOT) tissue wedge preparation. The RVOT region is identified on the epicardial and the endocardial surfaces (marked with a white dotted rectangle). **C**, Study protocol that includes group 1 (n=7) and group 2 (n=6) hearts. Group 1 experiments focused on evaluating the effects of sympathetic (isoproterenol [Iso], 100 nM) and parasympathetic stimulation (100 μM) in isolation. Group 2 experiments focused on evaluating the effect of parasympathetic stimulation post-sympathetic stimulation. Arrhythmia induction was attempted in all hearts using the S1S1 protocol or 50 Hz burst pacing. **D**, Bar graph depicting breakdown of the 30 donor hearts by sex, age, body mass index (BMI), and type of study. Ach indicates acetylcholine; Endo, endocardial; Epi, epicardial; LAA, left atrial appendage; LV, left ventricle; PA, pulmonary artery; RAA, right atrial appendage; RV, right ventricle; and TC, tissue chamber.

front collision was defined as a phenomenon wherein 2 wave fronts collided with each other and merged into a single wave front (Video S1). Wave front fractionation was defined as a phenomenon where a single wave front would split into 2 wave fronts (Video S2). A collision or a fractionation (wave front splitting) marked the end of the life span of a wave front. Alternately, wave front tracking was also terminated if the wave front moved past the field of view, fell below the 20-pixel threshold, or expired (Video S3). Wave fronts were also tracked for multiplicity and repeatability.[29] Multiplicity was defined as an index of number of unique wave front pathways in an overall activation pattern. Repeatability was defined as measure of the number of times a wave front propagation over a pathway was repeated (Video S4). PSs were calculated as nonzero topological charges constrained to the isophase wave fronts within 3-pixel radius (≈2 mm) in each frame. PS meandering (total distance traveled) and PS displacement (shortest path between the initial and final positions) were calculated by tracking individual PS trajectories across their life spans. To explore the endocardial-epicardial arrhythmia dissociation dynamics, wave fronts and PSs between the two surfaces were compared using spatiotemporal autocorrelation analysis. Epicardial and endocardial DF, regularity index, and organization index were also compared at each pixel location to compute the Jaccard similarity index.[30]

ELECTRICAL CARDIAC MAPPING

To establish the clinical relevance of optical mapping, we applied simultaneous electrical and optical cardiac mapping in donor hearts (n=3; male, 2; female, 1). Briefly, 2 stretchable passive electrode arrays were used for epicardial and endocardial electrical mapping. Each array (3×4 cm) had 64 electrodes arranged in an 8×8 matrix with interelectrode distance of ≈3 to 4 mm and electrode diameter of ≈1 mm. Fabrication of the electrode array was done at the Northwestern University as described ealier.[31] A custom-printed circuit board was fabricated at the Duke University[32] for connecting the electrode array to a data acquisition system (1024-channel RHD recording system; Intan Technologies, CA). The electrical and optical data acquisition systems were compared with enable synchronized measurements of electrical and optical signals. All the unipolar electrical signals were

processed in MATLAB, version 2020a. The local activation times were determined by calculating the time of dV/dt_{min}, which corresponds to the steepest downward slope in the activation complex. The local repolarization times were determined by calculating T_{up}—the point in the T wave with the maximum upward slope (Figure S2C). Activation recovery interval—a surrogate marker of APD—was then computed as the interval between local activation and repolarization time[33] and is assumed to occur near APD at 50% repolarization.[34]

Transcriptome

Tissues from human RVOT and RV apical region (RVAR), separated into epicardium and endocardium (total hearts, 10; male, 5; female, 5; 4 tissue samples from each heart) were collected for subsequent RNA extraction. RNA sequencing was performed with Illumina HiSeq using paired-end 150 reads (Novogene). DESeq2 was used for differential gene expression.[35] Differentially expressed gene cutoff was at $P_{adj}<0.05$. Enrichment analysis on differentially expressed genes was performed with goana[36] for gene ontology and clusterProfiler[37] for Kyoto Encyclopedia of Genes and Genomes.

Immunostaining

Briefly, fixed specimens of the human heart RVOT were shipped to the Eastern Tennessee State University at 4 °C in PBS containing 20% sucrose and 0.02% sodium azide. Slide-mounted tissue sections were immunostained at room temperature for specific neural markers using standard methods of ABC immunohistochemistry. Primary antibodies used included rabbit anti-VAChT (vesicular acetylcholine transporter; Synaptic Systems; catalog number 139103; 1:500), sheep anti-TH (tyrosine hydroxylase; Millipore; catalog number AB1542; 1:500), or rabbit anti-PGP9.5 (protein gene product 9.5; Abcam; catalog number ab108986; 1:2000). Nerve density was calculated as the area occupied by nerves as a percentage of the entire image area and reported as %area. Data was analyzed and graphed using Prism, version 8.4.3 (GraphPad Software, CA).

Statistical Analysis

All means characterizing the spatial average of a single study are represented as sample mean±SD. All means that characterize average trends across the cohort of donor hearts are reported as sample mean±SEM. Repeated measures ANOVA (1 or 2 way) with multiple comparisons and post hoc Holm-Sidak or Tukey Honest Significant Difference multiple comparison test was used for APD and PVC comparisons, respectively. Two-tailed paired *t* test was used for comparison between epicardial and endocardial wave fronts and PS metrics. Significance was defined as $P<0.05$.

RESULTS

Cardiac Mapping of Human RVOT Reveals Transmural APD and Repolarization Gradient

To determine whether the RVOT had distinctive electrophysiological features relative to the RVAR, we conducted cardiac mapping studies using RV tissue from 16 donor human hearts. The epicardial and endocardial activation, repolarization (repolarization time at 80% repolarization), and APD maps, as well as sample optical action potentials from a representative donor heart (D11) paced at 60 beats per minute (Figure 2A), depict the underlying repolarization dispersion and APD dispersion. For 3 donor hearts, we also conducted simultaneous electrical and optical mapping studies to evaluate the feasibility of dual modality mapping. The representative (D14) activation maps from simultaneous electrical and optical mapping paced at 120 beats per minute showed a similar profile (Figure 2B). Moreover, the activation recovery interval calculated from time-aligned electrograms correlated with APD at 50% repolarization (epicardium, r=0.81; endocardium, r=0.92; Pearson correlation). There was no statistically significant difference between the activation recovery interval and the APD at 50% repolarization restitution curves (Figure S3). These data suggest that simultaneous electrical and optical mapping can be used as a viable technique to generate a richer set of strongly correlated data. The APD80 restitution curves provide a statistical summary for each region (RVOT or RVAR), as well as the overall RV in the epicardium and the endocardium (Figure 2C). We noted shorter action potentials in the RVOT relative to the RVAR ($P_{epi}<0.0001$ and $P_{endo}<0.0001$, repeated measures 2-way ANOVA). We also found shorter APs in the RVOT epicardium relative to the RVOT endocardium ($P=0.0016$, repeated measures 2-way ANOVA). Moreover, there was a general trend with female APD80 being longer than male APD80, especially at lower heart rates; however, it was not statistically significant. Similarly, while the female repolarization time at 80% repolarization dispersion and APD80 dispersion trended to be longer than the male counterparts, they were not statistically significant. These results suggest that RVOT drives the transmural dispersion of repolarization and the transmural APD dispersion under normal physiological conditions.

Cholinergic Stimulation Attenuates Effects of Adrenergic Stimulation

To determine the role of parasympathetic stimulation in ventricular electrophysiology, we compared the electrophysiological response of RV subjected to acetylcholine

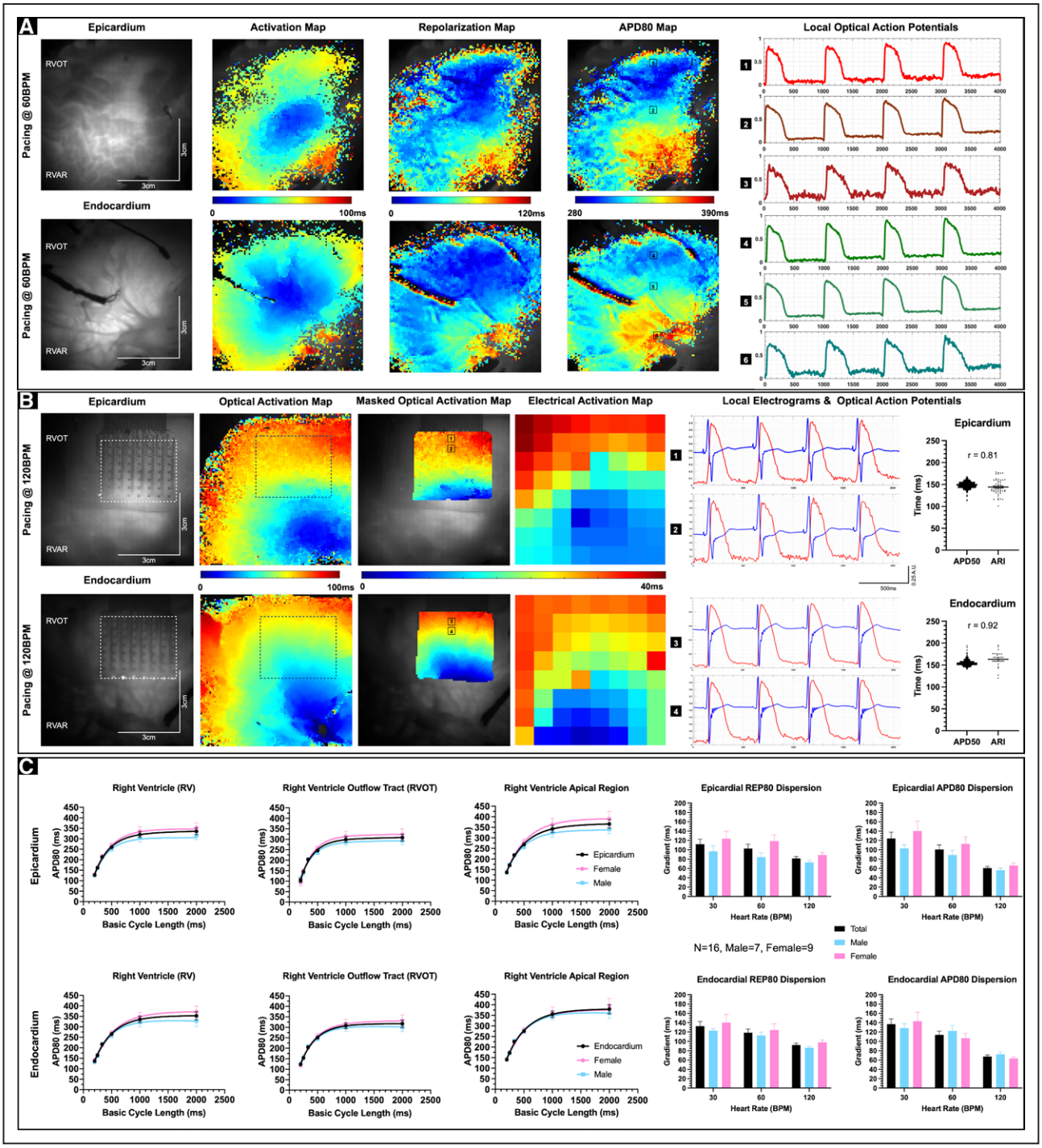

Figure 2. Baseline electrophysiology of donor human right ventricular outflow tract (RVOT).
A, Representative epicardial and endocardial activation, repolarization, and action potential duration at 80% repolarization (APD80) maps from a group 2 donor human heart (D11) paced at 60 beats per minute (BPM). Sample optical action potentials from the RVOT, right ventricular (RV) mid wall, and RV apical region are also shown. **B**, Representative epicardial and endocardial activation maps from simultaneous optical and electrical recording in a group 2 donor human heart (D14) paced at 120 BPM. Corresponding time-aligned optical action potential and local electrograms from the RVOT region are also shown. Box plot shows correlation between APD50 and activation recovery interval (ARI) calculated from the local optical and electrical signals in the epicardial (R^2=0.65, Pearson correlation) and endocardial regions (R^2=0.84, Pearson correlation). **C**, Baseline restitution curves from the RV, RVOT, and RV apical epicardial and endocardial regions are shown (n=16; male, 7 and female, 9). Female donor hearts trended to have relatively longer APD80 compared with male donor hearts, though not statistically significant. Representative epicardial and endocardial repolarization (repolarization time at 80% repolarization) and APD80 gradients at 30, 60, and 120 BPM are also shown. Females trended to have larger repolarization and APD80 gradients but not statistically significant.

(100 μM) treatment in the absence of sympathetic stimulation (group 1) with the electrophysiological response of RV pretreated with isoproterenol (100 nmol/L) and subsequently subjected to acetylcholine (100 μM) stimulation (group 2). In group 1 donor hearts, treatment with acetylcholine had no effect on APD relative to baseline conditions. Moreover, after acetylcholine was washed out, treatment with isoproterenol shortened APD as expected (Figure 3A; Figure S4A). In comparison, group 2 donor hearts were treated with isoproterenol first, which resulted in shortening of APD. However, while still under the influence of isoproterenol, additional treatment with acetylcholine resulted in prolongation of the APD (P_{epi}=0.015 and P_{endo}=0.029, repeated measures 2-way ANOVA) back toward baseline conditions (Figure 3B; Figure S4B). APD80 maps (paced at 60 beats per minute) and the corresponding sample optical action potentials from a representative group 2 donor heart (D11) highlight the initial shortening of APs in response to isoproterenol (100 nmol/L) stimulation and subsequent lengthening of APs reverting to near baseline conditions, upon treatment with acetylcholine (100 μM; Figure 3C). We also counted nerve density distribution in RVOT tissue samples from 4 additional donor hearts using immunohistochemical staining, which showed the presence of VAChT-positive, PGP9.5-positive, and TH-positive nerve densities in both the subepicardial and the subendocardial regions (Figure 3D; Figure S5).

Given that adrenergic stimulation promotes PVCs, it is possible that additional cholinergic stimulation could have

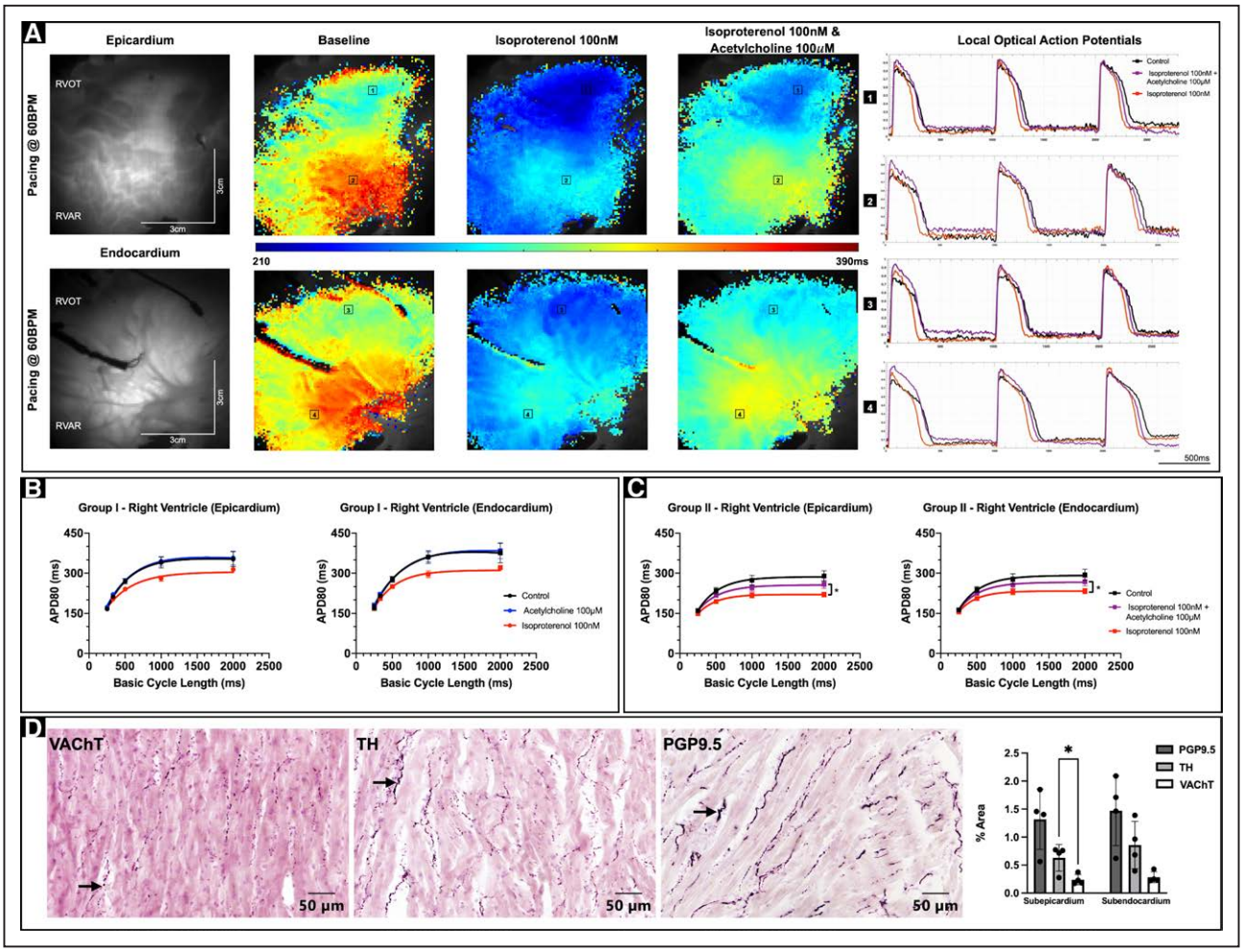

Figure 3. Effect of parasympathetic and sympathetic stimulation on action potential duration at 80% repolarization (APD80). **A**, Representative epicardial and endocardial APD80 maps from group 2 donor human heart (D11) paced at 60 beats per minute (BPM) under baseline conditions, after treatment with isoproterenol (100 nm) and finally after acetylcholine (100 μM) intervention in the presence of isoproterenol. Corresponding optical action potentials from 2 locations in the RVOT and RV mid wall are also shown. **B**, Epicardial and endocardial APD80 restitution curves from group 1 hearts, where the effects of sympathetic and parasympathetic stimulation were evaluated separately. While sympathetic stimulation shortened APD80, parasympathetic stimulation by itself had no effect on APD80. **C**, Epicardial and endocardial APD80 restitution curves from group 2 hearts, where the effect of parasympathetic stimulation was evaluated in the presence of sympathetic stimulation. Acetylcholine attenuated the effects of isoproterenol with the recovery of APD80 trending toward baseline conditions (P<0.05, repeated measures 2-way ANOVA). **D**, Immunostaining of RVOT tissue sample from representative donor human heart (D28) shows the presence of VAChT (vesicular acetylcholine transporter)-positive, PGP9.5 (protein gene product 9.5)-positive, and TH (tyrosine hydroxylase)-positive nerve densities in both the subepicardial and the subendocardial regions.

inverse effects on PVCs as seen previously with APD. To investigate further this idea, we tracked the frequency of PVCs in donor hearts from both groups (Figure 4A). In group 1, acetylcholine (100 μM) by itself had no effect on the frequency of PVCs compared with baseline. In contrast, treatment with isoproterenol (100 nmol/L) after washout of acetylcholine noticeably increased the frequency of PVCs (P=0.036, ordinary ANOVA). In group 2 hearts, initial treatment with isoproterenol (100 nmol/L) increased the frequency of PVCs (P=0.003, ordinary ANOVA), as expected. However, additional treatment with acetylcholine (100 μM) reduced the frequency of PVCs (P=0.034, ordinary ANOVA). The effects were consistent across both male and female donor hearts from both groups. However, we did not find any statistically significant sex-related differences in frequency of PVCs in response to either sympathetic or parasympathetic stimulation, presumably due to age of the hearts studied. Taken together, these results show that while parasympathetic stimulation by itself has no statistically significant effect on ventricular electrophysiology, in the presence of adrenergic stimulation, cholinergic stimulation attenuates the effects on APD and PVC frequency.

To investigate the nature of arrhythmia susceptibility, RV tissue from 13 donor hearts was treated with isoproterenol (100 nmol/L) and then subjected to S1S1 restitution stimulation to induce arrhythmias, which also triggered concordant or discordant alternans, dependent on the frequency of stimulation. An example of discordant APD at 50% repolarization alternans (Figure 4B) induced at 240 beats per minute from a representative donor heart (D10) and an example of concordant alternans (Figure S6A) induced at 300 beats per minute from another representative donor heart (D11) highlights the heterogeneous spatial distribution of alternans. In general, alternans appeared slightly more prevalent in the endocardium in comparison with the epicardium. Incidences of concordant alternans were relatively more frequent than discordant alternans (Figure S6B). Moreover, discordant alternans occurred at higher frequencies in comparison with concordant alternans. Finally, the RVOT region appeared to be slightly more susceptible to the alternans in comparison with the rest of the RV. Our data suggest that RVOT is susceptible to both concordant and discordant alternans, which may be linked to the intrinsic transmural dispersion of repolarization, as well as transmural APD dispersion, and result in vulnerability to arrhythmias.

Arrhythmia Wave Front and PS Dynamics

To get further insight into the transmural dynamics of RV arrhythmias, RV tissue was subjected to pharmacological arrhythmia promotion in combination with S1S1 protocol and, failing that, a 50-Hz burst pacing protocol. We induced sustained arrhythmias (lasting >15 minutes) in 12 donor hearts with 3 of them categorized as monomorphic ventricular tachycardia (MMVT). Representative arrhythmia phase data from donor heart (D14) showed reentrant MMVT and was characterized by a scroll wave, anchored by 2 PSs, one each on the epicardium and the endocardium, respectively (Figure 5A; Video S5). The DF (epicardium, 6.98±1.13 Hz; endocardium, 7.12±0.67 Hz), regularity index (epicardium, 0.75±0.18; endocardium, 0.78±0.14), and organization index (epicardium, 0.83±0.16; endocardium, 0.90±0.14) maps reflected organized nature of MMVT (Figure 5B). Arrhythmic wave fronts were characterized by collisions (epicardium, 28.77%; endocardium, 23.77%) and fractionations (epicardium, 27.10%; endocardium, 25.85%) but also showed a high degree of repeatability (epicardium, 67.95%; endocardium, 82.72%; Figure 5C). The average wave front size was larger, but the average wave front duration was smaller in the epicardium (size, 4.29±4.11 cm; duration, 4.3±7.7 ms) in comparison with the endocardium (size, 3.64±3.09 cm; duration, 6.5±10.2 ms). Moreover, the number of wave fronts was also larger in the epicardium (epicardium, 8.55/cm^{2}s; endocardium, 5.06/cm^{2}s). Analysis of epicardial and endocardial PS showed that the average duration of PS was larger in the endocardium (epicardium, 37.3±27.3 ms; endocardium, 43.8±28.8 ms; Figure 5D). Moreover, only a small fraction of PS was considered stable, defined as lasting at least one cycle length in duration (epicardium, 2.25%; endocardium, 2.01%). PS meandering (epicardium, 1.36±0.72 cm; endocardium, 1.31±0.68 cm) was slightly longer in the epicardium. Spatiotemporal autocorrelation analysis showed weak positive association between epicardial and endocardial wave fronts (28.4% of wave fronts followed similar trajectories) and PS (38.5% similar trajectories; Figure 5E). Dynamic time warp was used to quantify the similarity between epicardial and endocardial wave front temporal sequences and showed relatively higher incongruence (dynamic time warp distance, 46) compared with during pacing (dynamic time warp distance, 5; Figure S7). Moreover, the local epicardial and endocardial DF was highly congruent (96.6% similar). These results suggest that MMVT in donor human RV/RVOT is driven by a relatively small number of highly repeatable wave fronts and PSs that are reentrant in nature and have a high degree of regularity.

Representative arrhythmia phase data from donor heart (D4) shows ventricular fibrillation (VF) also with an instance of scroll wave (Figure 6A; Video S6). The DF (epicardium, 6.96±4.81 Hz; endocardium, 8.54±3.61 Hz), regularity index (epicardium, 0.32±0.17; endocardium, 0.38±0.15), and organization index (epicardium, 0.45±0.17; endocardium, 0.48±0.22) maps reflected the relatively less organized VF wave fronts in comparison with that seen in MMVT (Figure 6B). Analysis of epicardial and endocardial wave fronts showed a high degree of multiplicity (epicardium, 71.11%; endocardium, 70.99%)

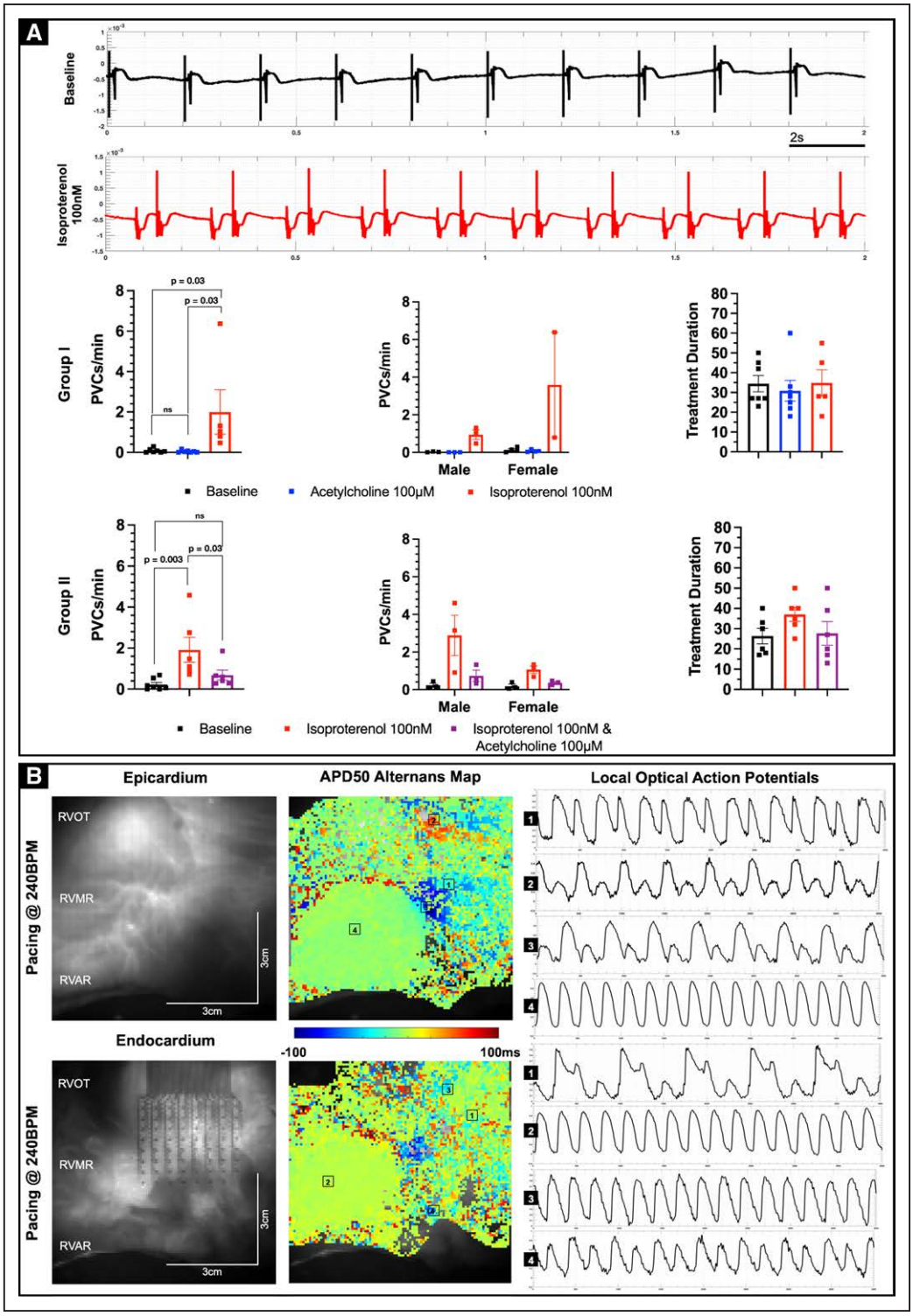

Figure 4. Effect of parasympathetic stimulation on arrhythmogenesis.

A, Representative tissue chamber bath ECG recordings under baseline conditions and after treatment with isoproterenol 100 nM from a representative group 2 donor heart (D11). Premature ventricular contractions (PVCs) were observed after the intervention as shown. In group 1 hearts, treatment with acetylcholine had no statistically significant effect on the frequency of PVCs relative to baseline conditions, whereas treatment with isoproterenol increased the frequency of PVCs (P=0.035, ordinary ANOVA). In group 2 hearts, acetylcholine intervention post-treatment with isoproterenol decreased the frequency of PVCs (P=0.034, ordinary ANOVA). Sex-related differences were not statistically significant. Treatment duration for each intervention across the two groups is also shown. **B**, Representative example of epicardial and endocardial action potential duration at 50% repolarization (APD50) maps depicting discordant alternans in the right ventricular outflow tract (RVOT) as a consequence of S1S1 arrhythmia induction protocol in group 1 donor human heart (D10). The alternans was triggered at the pacing rate of 240 beats per minute (BPM). Corresponding sample optical action potentials from 4 different locations in the epicardial and endocardial regions are also shown. RVAR indicates right ventricular apical region; and RVMR, right ventricle mid region.

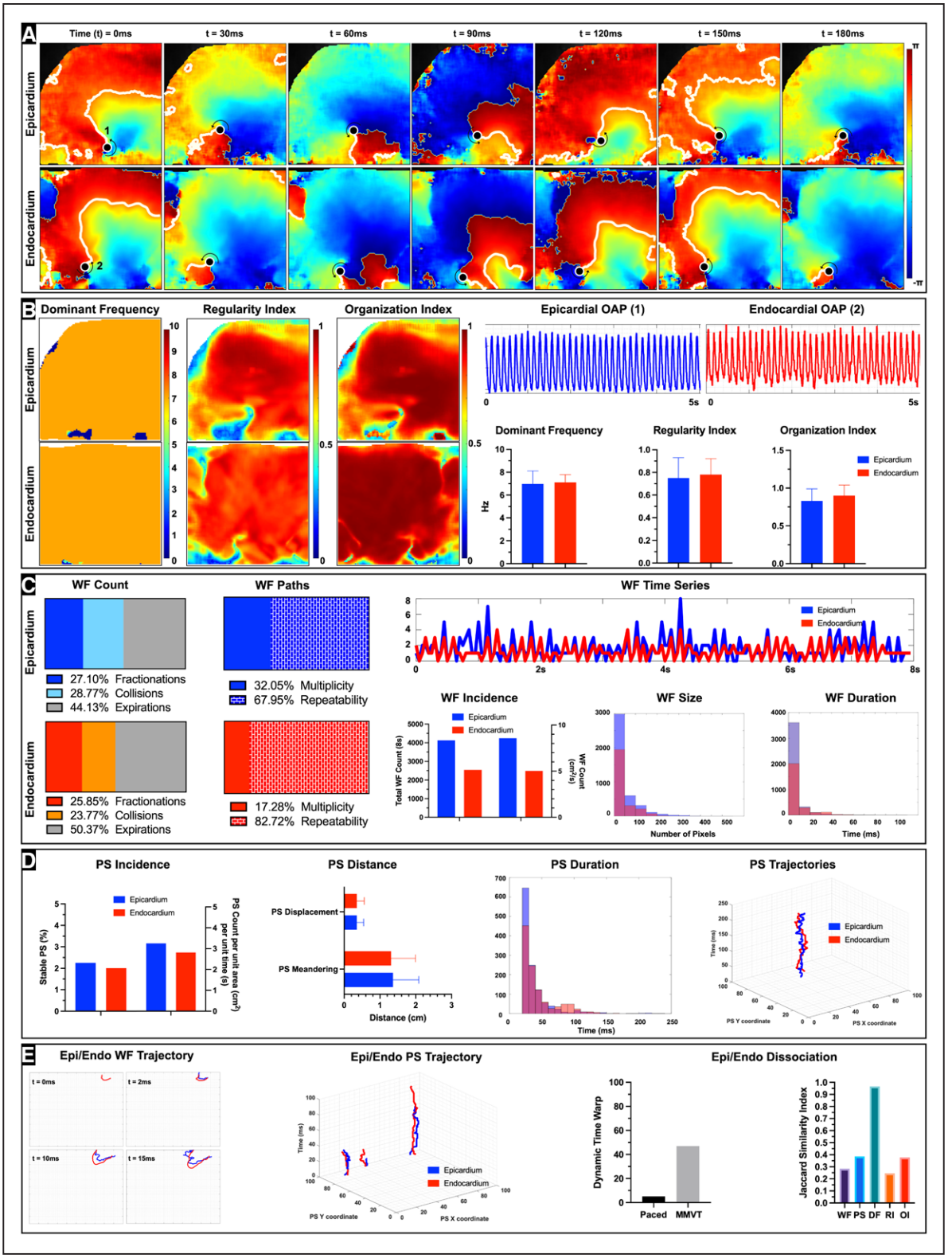

Figure 5. Monomorphic ventricular tachycardia (MMVT) dynamics.
A, Representative epicardial (Epi) and endocardial (Endo) spatiotemporal phase maps depicting reentrant MMVT in the donor human heart (D14) are shown. We can track the phase singularities (marked as a black dots) on both the Epi and Endo surfaces as the wave fronts complete one rotation (reentry) around the phase singularity (PS; rotor) over the duration of 180 ms. **B**, Epi and Endo dominant frequency (DF), regularity index (RI), and organization index (OI) maps along with the bar graphs are shown. Representative action potentials depicting MMVT from Epi (1) and Endo (2) locations are also shown. **C**, Wave front dynamics including breakdown of Epi and Endo wave fronts by percentage of wave fronts that terminated in collisions, fractionations, or otherwise expired are shown. (*Continued*)

Figure 5 Continued. We also show the percentage of Epi and Endo wave fronts that were characterized as unique (multiplicity) or repeating (repeatability). Given that this arrhythmia exhibited MMVT characteristics, we see a relatively higher percentage of wave front repeatability compared with other types of arrhythmias (eg, VF). Epi and Endo wave front (WF) time series shows the relative congruence in the number of wave fronts incident on both surfaces at a given point of time. Dynamic time warp (DTW) was used to quantify the similarity between the two temporal sequences. Total number of wave fronts tracked over the duration of 8 s as well as the number of wave fronts per unit area (cm^2) and per unit time (s) are shown. We also show a histogram of wave front size in pixels (1 pixel, ≈0.07 cm) and a histogram of wave front duration in milliseconds. **D**, Phase singularity (rotor) dynamics including the total number of PS tracked over the duration of 8 s, as well as the number of PS per unit area (cm^2) and per unit time (s) are shown. Bar graphs of PS displacement (minimum distance between the starting location of the PS and location just before PS termination) and PS meandering (total path length traversed by the PS over its life span) along with a histogram of PS duration in milliseconds are shown. We also show a sample Epi and Endo PS trajectory. **E**, Epi and Endo dissociation dynamics included spatiotemporal autocorrelation analysis of wave fronts and PS. A representative example of Epi and Endo wave front with similar trajectory over their first 15 ms is shown. Likewise, representative examples of 3 Epi and Endo PS with similar trajectories are also shown. Plot of the DTW values during pacing (120 beats per minute) and during arrhythmia are shown. The relatively higher number denotes larger dissimilarity between the temporal sequences of Epi and Endo arrhythmic wave fronts in comparison to when the tissue was paced. Jaccard similarity index was used to quantify similarity between Epi and Endo wave fronts, phase singularities, DF, RI, and OI. OAP indicates optical action potential.

and lower degree of repeatability (epicardium, 28.89%; endocardium, 29.01%) in comparison with MMVT (Figure 6C). The average size was larger, but the average duration was smaller in the epicardial wave fronts (size, 3.44±2.95 cm; duration, 3.71±5.98 ms) in comparison with the endocardial wave fronts (size, 3.10±2.28 cm; duration, 4.80±7.35 ms). Moreover, the number of wave fronts was also larger in the epicardium (epicardium, 19.59/cm^2s; endocardium, 15.84/cm^2s), and both were larger than compared with MMVT wave fronts. Analysis of epicardial and endocardial PS showed that the average duration of PS was also larger in the endocardium (epicardium, 33.4±17.98 ms; endocardium, 38.97±24.57 ms; Figure 6D). In addition, relatively smaller fraction of PS was stable (epicardium, 0.61%; endocardium, 1.48%) in comparison with MMVT. PS meandering (epicardium, 1.28±0.64 cm; endocardium, 1.15±0.66 cm) and displacement (epicardium, 0.35±0.21 cm; endocardium, 0.33±0.19 cm) were also longer in the epicardium. Spatiotemporal autocorrelation analysis showed weaker positive association between the epicardial and endocardial wave fronts (16.5% of wave fronts followed similar trajectories) and PS (33.17% similar trajectories) in comparison with MMVT (Figure 6E). These results suggest that VF in donor human RV/RVOT is driven by a relatively larger number of irregular and less organized wave fronts and PSs that still appear to be reentrant in nature.

The statistical summary of arrhythmia dynamics from 12 donor hearts suggests that the endocardial arrhythmic wave fronts are relatively more regular (P=0.0026, paired t test) and organized (P=0.0058, paired t test) than that seen in the epicardium (Figure 7B and 7C). However, we do not observe any statistically significant sex-specific differences relative to arrhythmia wave front organization (Figure S8B and S8C). Epicardial wave front size is larger (P=0.0034, paired t test) and so is wave front count (P=0.0003, paired t test) in comparison with endocardial wave fronts (Figure 7D and 7E), whereas the endocardium is characterized by longer wave front duration (P=0.0001, paired t test; Figure 7F). Moreover, epicardial wave fronts are characterized more fractionations in comparison with the endocardium (Figure 7G). PS duration (P<0.0001, paired t test) is longer in the endocardium than seen in the epicardium (Figure 7L), whereas the epicardium is characterized by larger PS meandering and displacement (Figure 7M and 7N). Taken together, these results provide further statistical evidence that the arrhythmia in the endocardium is relatively more organized than in the epicardium.

Sex-Specific Differences in the Human RVOT Transcriptome

We sought to get insight into the regulatory features of the RVOT by determining the transcriptome profile of RVOT and RVAR tissue from 10 donor human hearts using bulk RNA sequencing. Principal component analyses showed that the tissue samples were clustered together by sex along the first principal component, which accounted for 26% of the observed variance (Figure 8A). Bioinformatic analysis showed that sex altered expression of 261 genes in the RVOT (Figure 8B). To further elucidate sex- and location-specific (RVAR versus RVOT, epicardium versus endocardium) differences, we performed hierarchical clustering of both genes and the samples based on the gene expression profile (differentially expressed genes) in the gene expression matrix, identifying the top 20 genes (Figure 8C). Further gene ontology analysis showed that these sex-regulated genes are mainly involved in immunoglobin complex and humoral immune response, etc, in case of females and demethylase activity and demethylation, etc, in case of males (Figure 8D). The Kyoto Encyclopedia of Genes and Genomes analysis revealed the top 16 Kyoto Encyclopedia of Genes and Genomes–annotated pathways enriched for differentially expressed genes expressed in male and female RVOT (Figure 8E). Among them, MAPK (mitogen-activated protein kinase) signaling,[38] calcium signaling,[39] and cGMP-PKG (protein kinase G) signaling[40] pathways, which were enriched in male RVOT, have been reported to be involved in cardiac hypertrophy and cardiac electrophysiological remodeling. Incidentally, neurodegeneration pathways were enriched in female RVOT. These differences were not as pronounced when

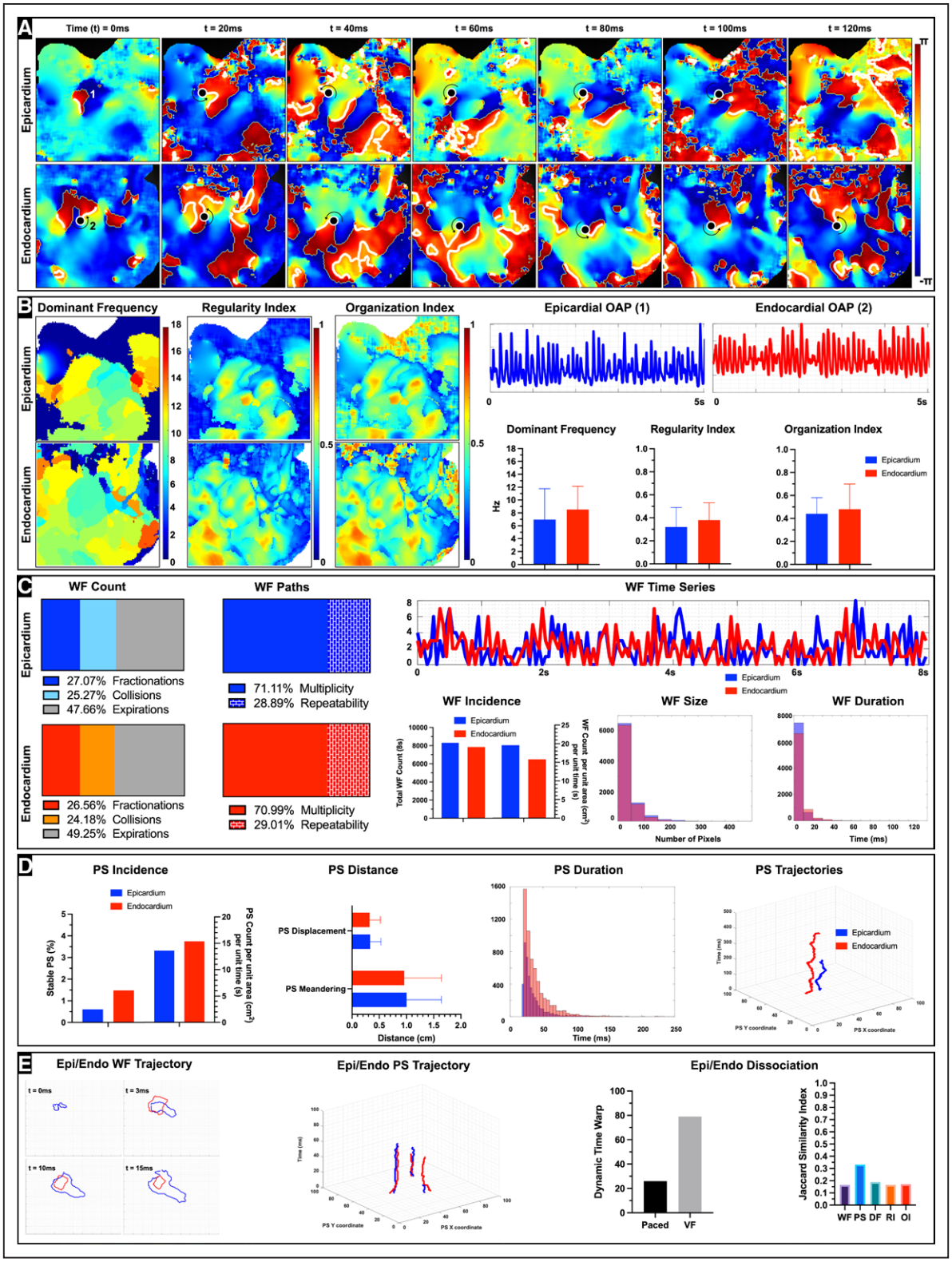

Figure 6. Ventricular fibrillation (VF) dynamics.

A, Representative epicardial (Epi) and endocardial (Endo) spatiotemporal phase maps depicting reentrant VF in the donor human heart (D4) are shown. We can track the phase singularities (marked as a black dots) on both the Epi and Endo surfaces. In this instance, we see the Endo wave front (WF) complete one rotation (reentry) around the phase singularity (PS; rotor) over the duration of 120 ms. **B**, Epi and Endo dominant frequency (DF), regularity index (RI), and organization index (OI) maps along with the bar graphs are shown and depict heterogeneity relative to that seen during MVT. Representative action potentials depicting VF from Epi (1) and Endo (2) locations are also shown. **C**, WF dynamics including breakdown of Epi and Endo WFs by percentage of WFs that terminated in collisions, (*Continued*)

Figure 6 Continued. fractionations, or otherwise expired are shown. We also show percentage of Epi and Endo WFs that were characterized as unique (multiplicity) or repeating (repeatability). Given that this arrhythmia exhibited VF characteristics, we see a relatively lower percentage of WF repeatability compared with other types of arrhythmias (eg, MMVT). Epi and Endo WF time series shows the relative congruence or lack thereof in the number of WFs incident on both surfaces at a given point of time. Dynamic time warp (DTW) was used to quantify the similarity between the two temporal sequences. Total number of WFs tracked over the duration of 8 s, as well as the number of WFs per unit area (cm^2) and per unit time (s) are shown. We also show a histogram of WF size in pixels (1 pixel, ≈0.07 cm) and a histogram of WF duration in milliseconds. **D**, Phase singularity (rotor) dynamics including total number of PS tracked over the duration of 8 s, as well as the number of PS per unit area (cm^2) and per unit time (s) are shown. Bar graphs of PS displacement (minimum distance between the starting location of the PS and location just before PS termination) and PS meandering (total path length traversed by the PS over its life span) along with a histogram of PS duration in milliseconds are shown. We also show a sample Epi and Endo PS trajectory. **E**, Epi and Endo dissociation dynamics included spatiotemporal autocorrelation analysis of WFs and PS. A representative example of Epi and Endo WF with similar trajectory over their first 15 ms is shown. Likewise, representative examples of 3 Epi and Endo PS with similar trajectories are also shown. Plots of the DTW values during pacing (120 beats per minute) and during arrhythmia are shown. The relatively higher number denotes larger dissimilarity between the temporal sequences of Epi and Endo arrhythmic WFs in comparison to when the tissue was paced. Jaccard similarity index was used to quantify similarity between Epi and Endo WFs, phase singularities, DF, RI, and OI. OAP indicates optical action potential.

comparing sex-specific differences in the RVAR (Figure S9). Our results suggest a trend that MAPK signaling, calcium signaling, and cGMP-PKG signaling pathways could be linked with the sex-specific electrophysiological differences seen in the RVOT.

DISCUSSION

In this study, we studied donor human hearts to assess the basic electrophysiology and transcriptome of human RVAR and RVOT tissue and investigate the effects of autonomic modulation on arrhythmia susceptibility, while also leveraging these data to characterize transmural arrhythmia dynamics. We showed that RVOT is characterized by shorter action potentials in comparison with the RVAR, which is evident in both transmural dispersion of repolarization and APD. We also showed that cholinergic stimulation in isolation has no effect on the RV electrophysiology. However, in the presence of adrenergic stimulation, additional cholinergic stimulation counteracts the sympathetic effects by attenuating both APD shortening and the frequency of PVCs. Finally, we also showed that RV arrhythmia dynamics is characterized by reentry, which is relatively more organized in the endocardium in comparison with the epicardium.

Our data support the existence of spatial heterogeneity in repolarization and APD between epicardial and endocardial RVOT and the RVAR under physiological conditions. The reasons for this heterogeneity remain unclear but could be associated with one or more of conduction velocity heterogeneities or spatial heterogeneities of calcium dynamics and the ionic currents in the sarcolemma that drive repolarization phase of action potentials or intercellular uncoupling. Work done by Boukens et al[10] in mice suggests that the slow conducting phenotype of the embryonic RVOT is maintained in adult heart resulting in lower conduction reserve in the RVOT relative to RV. Our transcriptomic analysis of RVAR and RVOT tissue did not reveal any statistically significant differences in the calcium, potassium, or gap junction channel expressions. However, work by Gaborit et al[41] on nondiseased human hearts suggests that basal epicardium is characterized by higher expression of genes related to calcium handling (Cav1.2 and SERCA2 [sarco-endoplasmic reticulum Ca2+ ATPase 2 an enzyme]), whereas the basal endocardium has higher expression of sodium channels (Nav1.5 and Navβ1). There is also literature evidence to suggest that in healthy human hearts, RV contains relatively larger collagen content and fat relative to the left ventricle.[3] Moreover, if nonvascular intramural clefts seen in the mouse RVOT[9] are present in the human RVOT, it could also facilitate subtle intercellular uncoupling. While the precise mechanisms remain unelucidated, our results encourage future studies to understand the specific role of each mechanism.

Our study showed that acetylcholine by itself had no effect on APD or the frequency of PVCs in the RV, unlike isoproterenol, which shortened APD and increased the frequency of PVCs. However, acetylcholine in the presence of adrenergic stimulation mediated reversal of isoproterenol shortened APD and decreased the frequency of PVCs induced by isoproterenol. Moreover, immunohistochemistry also confirmed ventricular cholinergic innervation, revealing the presence of VAChT nerve densities across the RVOT transmural wall. Vagal nerve stimulation has been reported in preclinical and clinical studies to have antiarrhythmic effects, especially in the setting of acute and chronic myocardial ischemia and infarction, which is often associated with imbalance in autonomic modulation in favor of sympathetic hyperactivity.[42–46] The presence of vagal innervation in the ventricle has been confirmed by others, and it has also been suggested that muscarinic receptors on adrenergic nerve terminals could attenuate norepinephrine release, resulting in parasympathetically mediated inhibitory effects on cardiac sympathetic activity.[47–49]

Our data also revealed that RV/RVOT is characterized by complex transmural arrhythmia dynamics that can extend from a relatively few organized and stable reentrant rotors as seen during MMVT to many disorganized and transient rotors, which also exhibited reentry as seen during VF. Compared with the endocardium, the epicardium had more wave fronts per unit area and per unit time and more wave front fractionations, which could be associated with the fat accumulation on the epicardial surface.

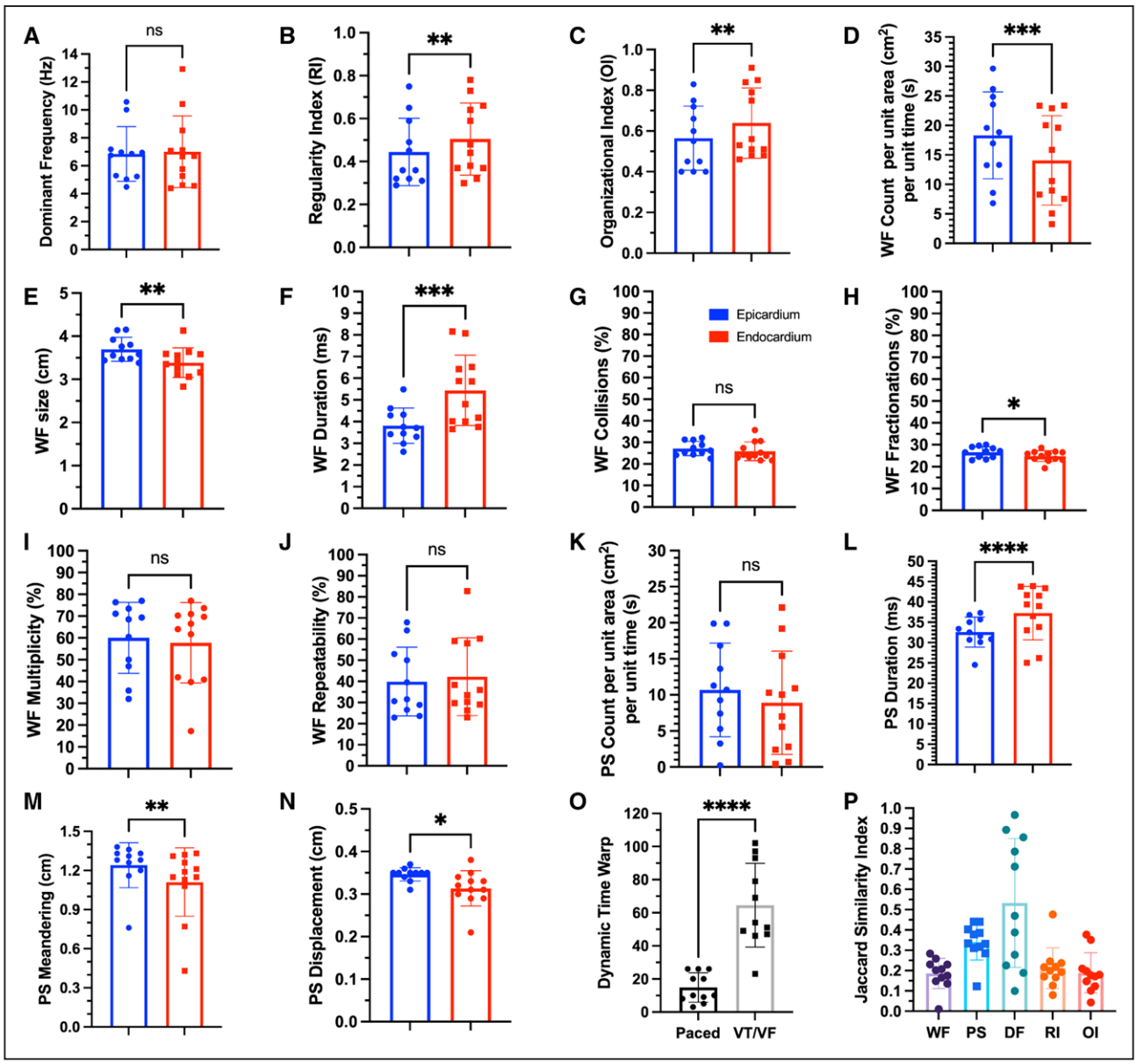

Figure 7. Statistical summary of arrhythmia dynamics.

A, Dominant frequency (DF) was not statistically different between the epicardium and endocardium. **B**, Regularity index (RI) was higher in the endocardium (P=0.0026, paired t test). **C**, Organization index (OI) was higher in the endocardium (P=0.0058, paired t test), suggesting that the arrhythmic wave fronts (WFs) were more regular and organized in the endocardium in comparison with the epicardium. **D**, Number of WFs per unit area per unit time were higher in the epicardium (P=0.0003, paired t test). **E**, Average size of the WFs was larger in the epicardium (P=0.0034, paired t test). **F**, Average duration of the WFs was longer in the endocardium (P=0.0001, paired t test). **G**, Percentage of WFs that terminated with collisions was not statistically different between the two surfaces. **H**, Percentage of WFs that terminated with fractionations (WF splitting into ≥2 WFs) was higher in the epicardium (P=0.0174, paired t test). **I**, Percentage of WFs that were unique (multiplicity) was not statistically different between the two surfaces. **J**, Percentage of WFs that repeated their trajectories (repeatability) was not statistically different between the two surfaces. **K**, Number of phase singularity (PS) per unit area per unit time was not statistically different between epicardium and endocardium. **L**, Average duration of PS was longer in the endocardium in comparison with epicardium (P<0.0001, paired t test). **M**, Average path length of the PS trajectory was longer in the epicardium (P=0.0093, paired t test). **N**, Average distance traveled by the PS was smaller in the endocardium in comparison with epicardium (P=0.0286, paired t test), suggesting that the PS was more spatially stable. **O**, The temporal sequences of arrhythmic WFs were more dissimilar than that of paced WFs as expected. **P**, There was weak positive spatiotemporal autocorrelation between epicardial and endocardial WFs and PS. Epicardial and endocardial local DF was more spatially correlated relative to local RI and local OI. VF indicates ventricular fibrillation; and VT, ventricular tachycardia.

However, the endocardium was characterized by longer wave front duration and PS duration, larger regularity and organizational index, and shorter PS meandering and PS displacement. Taken together, these metrics suggest that the endocardium has relatively more organized and stable arrhythmia dynamics relative to the epicardium. The relative disorganization of arrhythmias on the epicardium could be associated with the accumulation of epicardial

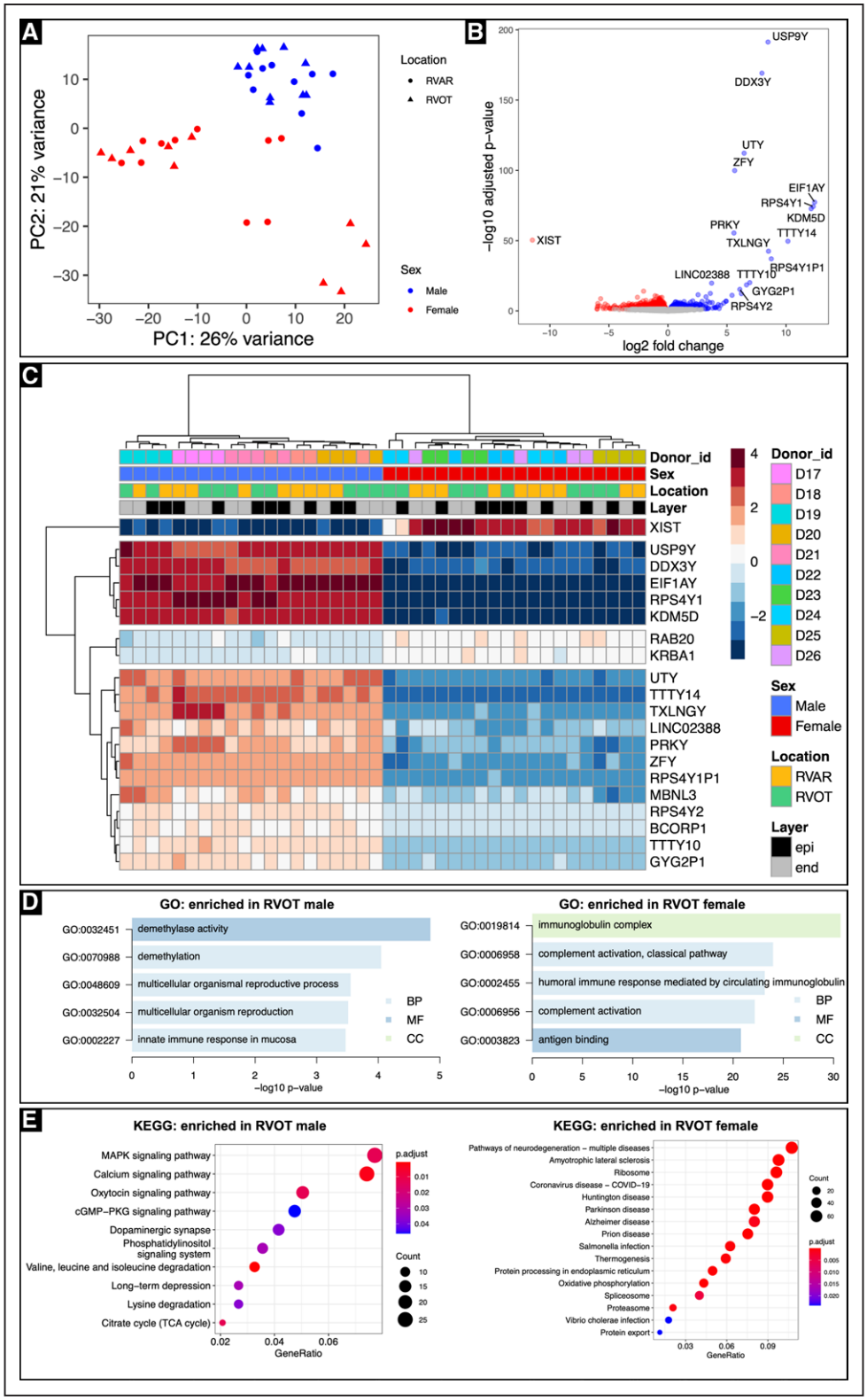

Figure 8. Transcriptome profiling of human right ventricular outflow tract (RVOT).
A, Principal component analyses showed that the tissue samples were clustered together by sex along the first principal component, which accounted for 26% of the observed variance. **B**, Volcano plot showing sex altered expression of 261 genes in the RVOT. **C**, Hierarchical clustering of both genes and the samples based on the gene expression profile (DEGs) in the gene expression matrix, identifying the top 20 genes. **D**, The gene ontology (GO) analysis suggests a trend that these sex-regulated genes are mainly involved in immunoglobin complex, humoral immune response, etc, in case of females and demethylase activity, demethylation, etc, in case of males. **E**, The Kyoto Encyclopedia of Genes and Genomes (KEGG) analysis revealed the top 16 KEGG-annotated pathways enriched for DEGs expressed in male and female RVOTs. BP indicates biological process; CC, cellular component; end, endocardial; epi, epicardial; MAPK, mitogen-activated protein kinase; MF, molecular function; PC, principal component; PKG, protein kinase G; RVAR, right ventricular apical region; and TCA, tricarboxylic acid cycle.

adipose tissue, which has been associated with electrical and structural remodeling in the atria.[50] In addition, there was a weak positive spatiotemporal association between epicardial and endocardial wave fronts and PS and could be characterized as 3-dimensional scroll waves with colocalized rotors extending out onto both surfaces. Our findings suggest reentry as the primary mechanism driving the arrhythmia dynamics in RV. In case of low-complexity arrhythmias such as MMVT, the reentrant arrhythmia appears to be characterized by a small number of stable rotors. Furthermore, in case of high-complexity arrhythmias such as VF, the reentrant arrhythmia appears to be driven by multiple propagating wavelets. Taken together, we believe the arrhythmia dynamics lie on a spectrum with stable reentrant rotors[21] governing low-complexity arrhythmias on one end and multiple wavelets[51] driving high-complexity fibrillation dynamics on the other end. Incidentally, the average displacement of the rotor (epicardium, 0.32±0.01 cm; endocardium, 0.31±0.02 cm) also suggests the minimal spatial resolution needed to accurately localize arrhythmia drivers.

VTs originating in the RVOT are commonly associated with focal mechanisms, including enhanced automaticity and cAMP-mediated triggered activity.[2] Moreover, the ectopic activity in the RVOT can be facilitated by catecholamines but seldom results in sustained VT, especially in nonpathological hearts. In our study, we combined infusion with isoproterenol with concurrent rapid pacing to achieve sustained VT. It is likely that in failing hearts, the ectopic activity is more likely to lead to sustained VT and will be investigated in the future.

Limitations

Our work presents several limitations. First, the cohort of donor hearts procured for this study had unavoidable high variability given the different comorbidities present (eg, hypertension, diabetes, asymptomatic onset of cardiovascular disease, perhaps due to age, etc). Most of the hearts we received were rejected for transplantation due to age restriction, and we had limited information available on the exact health status. As such, we cannot discount the effect of comorbidities that may be present. Even so, the donor hearts represent as close to normal human physiology as is possible in a basic research setting. Second, the fat accumulation on the epicardium and the presence of endocavitary structures (eg, papillary muscles, moderator band, and trabeculations) made it difficult to measure conduction velocity with precision. Therefore, the role of conduction velocity heterogeneity was not explored. Third, we did not quantify the fibrous and fatty infiltration or the number of nonvascular clefts in the RVOT tissue, which could potentially play a role in the spatial heterogeneities of APD and repolarization. Fourth, we did not investigate the role of Purkinje fibers in the arrhythmia dynamics, which could contribute to arrhythmia through a combination of triggered activity and reentrant wave fronts.[52] Fifth, recent studies[53,54] have suggested that idiopathic VF seen in structurally normal hearts may result from structural abnormalities including diffuse fibrosis and increased collagen content in the myocardium that may not be readily detected by standard clinical imaging modalities. While the donor hearts used in this study may have developed age-related fibrosis, we did not explore the role of subtle structural abnormalities in arrhythmogenesis.

Conclusions

In this report, we show that human RVOT electrophysiology is characterized by shorter action potentials relative to the RVAR resulting in spatial heterogeneity of repolarization and APD and potentially creating a substrate for arrhythmia vulnerability. We also report that cholinergic stimulation attenuates the arrhythmogenic effect of adrenergic stimulation by reversing APD shortening and decreasing the frequency of PVCs. Finally, we also show that RV arrhythmia is characterized by reentry associated with a small but stable group of rotors as seen in MMVT or multiple transient wavelets as seen in VF. Furthermore, the epi/endo arrhythmia dynamics is characterized by weak positive spatial-temporal autocorrelation between epicardial and endocardial wave fronts and rotors that are relatively more organized and stable in the endocardium.

ARTICLE INFORMATION

Received October 12, 2021; accepted February 17, 2022.

Affiliations

Department of Biomedical Engineering, George Washington University, Washington, DC (K.A., A.G., N.R.F., J.B., K.G., I.R.E.). Institut de rhythmologie et de modélisation cardiaque (LIRYC; The Rhythmology and Heart Modeling Institute), Bordeaux University, France (N.R.F., O.B.). Department of Biomedical Engineering, Northwestern University, Evanston, IL (J.L., J.A.R.). Department of Electrical and Computer Engineering, University of Illinois at Urbana-Champaign (Y.Z.). Department of Biomedical Engineering, Duke University, Durham, NC (C.-H.C., J.V.). Department of Biomedical Sciences, East Tennessee State University, Johnson City (E.H.S., M.D.P., J.C., D.B.H.). University of California at Los Angeles Cardiac Arrhythmia Center and Neurocardiology Research Program of Excellence, University of California, Los Angeles (P.H., S.M., O.A.A., K.S.). Department of Materials Science and Engineering, Ohio State University, Columbus, OH (J.L.).

Acknowledgments

We thank Allan Li, Brianna Cathey, Sharon George, Rose Yin, Zach Li, Micah Madrid, and Istvan Koncz for their excellent technical assistance.

Sources of Funding

This work was supported by the National Institutes of Health (NIH) to Drs Efimov and Aras (R44 HL139248, 3OT2OD023848, and 1K99HL148523-01A1), the NIH to Dr Hanna (F32HL152609), the American Heart Association 2019 CENTER Arrhythmias SCD Strategically Focused Research Network to Dr Efimov, and the Leducq Foundation grant RHYTHM to Dr Efimov.

Disclosures

None.

Supplemental Material

Supplemental Materials
Supplemental Methods
Figures S1–S9
Videos S1–S6

REFERENCES

1. Blok M, Boukens BJ. Mechanisms of arrhythmias in the brugada syndrome. *Int J Mol Sci.* 2020;21:E7051. doi: 10.3390/ijms21197051
2. Lerman BB, Cheung JW, Ip JE, Liu CF, Thomas G, Markowitz SM. Mechanistic subtypes of focal right ventricular tachycardia. *J Cardiovasc Electrophysiol.* 2018;29:1181–1188. doi: 10.1111/jce.13505
3. Miles C, Westaby J, Ster IC, Asimaki A, Boardman P, Joshi A, Papadakis M, Sharma S, Behr ER, Sheppard MN. Morphometric characterization of collagen and fat in normal ventricular myocardium. *Cardiovasc Pathol.* 2020;48:107224. doi: 10.1016/j.carpath.2020.107224
4. Basso C, Thiene G. Adipositas cordis, fatty infiltration of the right ventricle, and arrhythmogenic right ventricular cardiomyopathy. Just a matter of fat? *Cardiovasc Pathol.* 2005;14:37–41. doi: 10.1016/j.carpath.2004.12.001
5. Ghonim S, Voges I, Gatehouse PD, Keegan J, Gatzoulis MA, Kilner PJ, Babu-Narayan SV. Myocardial architecture, mechanics, and fibrosis in congenital heart disease. *Front Cardiovasc Med.* 2017;4:30. doi: 10.3389/fcvm.2017.00030
6. Asirvatham SJ. Correlative anatomy for the invasive electrophysiologist: outflow tract and supravalvar arrhythmia. *J Cardiovasc Electrophysiol.* 2009;20:955–968. doi: 10.1111/j.1540-8167.2009.01472.x
7. De Almeida MC, Stephenson RS, Anderson RH, Benvenuti LA, Loukas M, Aiello VD. Human subpulmonary infundibulum has an endocardial network of specialized conducting cardiomyocytes. *Heart Rhythm.* 2020;17:123–130. doi: 10.1016/j.hrthm.2019.07.033
8. Kamakura S, Shimizu W, Matsuo K, Taguchi A, Suyama K, Kurita T, Aihara N, Ohe T, Shimomura K. Localization of optimal ablation site of idiopathic ventricular tachycardia from right and left ventricular outflow tract by body surface ECG. *Circulation.* 1998;98:1525–1533. doi: 10.1161/01.cir.98.15.1525
9. Kelly A, Salerno S, Connolly A, Bishop M, Charpentier F, Stølen T, Smith GL. Normal interventricular differences in tissue architecture underlie right ventricular susceptibility to conduction abnormalities in a mouse model of Brugada syndrome. *Cardiovasc Res.* 2018;114:724–736. doi: 10.1093/cvr/cvx244
10. Boukens BJ, Sylva M, de Gier-de Vries C, Remme CA, Bezzina CR, Christoffels VM, Coronel R. Reduced sodium channel function unmasks residual embryonic slow conduction in the adult right ventricular outflow tract. *Circ Res.* 2013;113:137–141. doi: 10.1161/CIRCRESAHA.113.301565
11. Ou B, Nakagawa M, Kajimoto M, Nobe S, Ooie T, Ichinose M, Yonemochi H, Ono N, Shimada T, Saikawa T. Heterogeneous expression of connexin 43 in the myocardium of rabbit right ventricular outflow tract. *Life Sci.* 2005;77:52–59. doi: 10.1016/j.lfs.2004.12.030
12. Zaitsev AV, Torres NS, Cawley KM, Sabry AD, Warren JS, Warren M. Conduction in the right and left ventricle is differentially regulated by protein kinases and phosphatases: implications for arrhythmogenesis. *Am J Physiol Heart Circ Physiol.* 2019;316:H1507–H1527. doi: 10.1152/ajpheart.00660.2018
13. Benoist D, Dubes V, Roubertie F, Gilbert SH, Charron S, Constantin M, Elbes D, Vieillot D, Quesson B, Cochet H, et al. Proarrhythmic remodelling of the right ventricle in a porcine model of repaired tetralogy of Fallot. *Heart.* 2017;103:347–354. doi: 10.1136/heartjnl-2016-309730
14. Morita H, Zipes DP, Lopshire J, Morita ST, Wu J. T wave alternans in an in vitro canine tissue model of Brugada syndrome. *Am J Physiol Heart Circ Physiol.* 2006;291:H421–H428. doi: 10.1152/ajpheart.01259.2005
15. Zhou P, Yang X, Li C, Gao Y, Hu D. Quinidine depresses the transmural electrical heterogeneity of transient outward potassium current of the right ventricular outflow tract free wall. *J Cardiovasc Dis Res.* 2010;1:12–18. doi: 10.4103/0975-3583.59979
16. Shivkumar K, Ardell JL. Cardiac autonomic control in health and disease. *J Physiol.* 2016;594:3851–3852. doi: 10.1113/JP272580
17. Fukuda K, Kanazawa H, Aizawa Y, Ardell JL, Shivkumar K. Cardiac innervation and sudden cardiac death. *Circ Res.* 2015;116:2005–2019. doi: 10.1161/CIRCRESAHA.116.304679
18. Machhada A, Marina N, Korsak A, Stuckey DJ, Lythgoe MF, Gourine AV. Origins of the vagal drive controlling left ventricular contractility. *J Physiol.* 2016;594:4017–4030. doi: 10.1113/JP270984
19. Pauziene N, Alaburda P, Rysevaite-Kyguoliene K, Pauza AG, Inokaitis H, Masaityte A, Rudokaite G, Saburkina I, Plisiene J, Pauza DH. Innervation of the rabbit cardiac ventricles. *J Anat.* 2016;228:26–46. doi: 10.1111/joa.12400
20. Ulphani JS, Cain JH, Inderyas F, Gordon D, Gikas PV, Shade G, Mayor D, Arora R, Kadish AH, Goldberger JJ. Quantitative analysis of parasympathetic innervation of the porcine heart. *Heart Rhythm.* 2010;7:1113–1119. doi: 10.1016/j.hrthm.2010.03.043
21. Jalife J. Ventricular fibrillation: mechanisms of initiation and maintenance. *Annu Rev Physiol.* 2000;62:25–50. doi: 10.1146/annurev.physiol.62.1.25
22. Tabereaux PB, Dosdall DJ, Ideker RE. Mechanisms of VF maintenance: wandering wavelets, mother rotors, or foci. *Heart Rhythm.* 2009;6:405–415. doi: 10.1016/j.hrthm.2008.11.005
23. Allessie MA, de Groot NM, Houben RP, Schotten U, Boersma E, Smeets JL, Crijns HJ. Electropathological substrate of long-standing persistent atrial fibrillation in patients with structural heart disease: longitudinal dissociation. *Circ Arrhythm Electrophysiol.* 2010;3:606–615. doi: 10.1161/CIRCEP.109.910125
24. Lou Q, Li W, Efimov IR. The role of dynamic instability and wavelength in arrhythmia maintenance as revealed by panoramic imaging with blebbistatin vs. 2,3-butanedione monoxime. *Am J Physiol Heart Circ Physiol.* 2012;302:H262–H269. doi: 10.1152/ajpheart.00711.2011
25. Aras KK, Faye NR, Cathey B, Efimov IR. Critical volume of human myocardium necessary to maintain ventricular fibrillation. *Circ Arrhythm Electrophysiol.* 2018;11:e006692. doi: 10.1161/CIRCEP.118.006692
26. Noda T, Shimizu W, Taguchi A, Aiba T, Satomi K, Suyama K, Kurita T, Aihara N, Kamakura S. Malignant entity of idiopathic ventricular fibrillation and polymorphic ventricular tachycardia initiated by premature extrasystoles originating from the right ventricular outflow tract. *J Am Coll Cardiol.* 2005;46:1288–1294. doi: 10.1016/j.jacc.2005.05.077
27. Orozco-Duque A, Ugarte JP, Tobón C, Morillo C, Saiz J, Bustamante J. Dominant frequency, regularity and organization indexes response to preprocessing filter variations on simulated electrograms during atrial fibrillation. In: BIOSIGNALS 2013 Proceedings of the International Conference on Bio-Inspired Systems and Signal Processing, Barcelona, Spain, February 11–14, 2013. 306–309.
28. Gutbrod SR, Walton R, Gilbert S, Meillet V, Jaïs P, Hocini M, Haïssaguerre M, Dubois R, Bernus O, Efimov IR. Quantification of the transmural dynamics of atrial fibrillation by simultaneous endocardial and epicardial optical mapping in an acute sheep model. *Circ Arrhythm Electrophysiol.* 2015;8:456–465. doi: 10.1161/CIRCEP.114.002545
29. Rogers JM, Usui M, KenKnight BH, Ideker RE, Smith WM. Recurrent wavefront morphologies: a method for quantifying the complexity of epicardial activation patterns. *Ann Biomed Eng.* 1997;25:761–768. doi: 10.1007/BF02684160
30. Levandowsky M, Winter D. Distance between sets. *Nature.* 1971;234:34-35.
31. Tian L, Zimmerman B, Akhtar A, Yu KJ, Moore M, Wu J, Larsen RJ, Lee JW, Li J, Liu Y, et al. Large-area MRI-compatible epidermal electronic interfaces for prosthetic control and cognitive monitoring. *Nat Biomed Eng.* 2019;3:194–205. doi: 10.1038/s41551-019-0347-x
32. Insanally M, Trumpis M, Wang C, Chiang CH, Woods V, Palopoli-Trojani K, Bossi S, Froemke RC, Viventi J. A low-cost, multiplexed μECoG system for high-density recordings in freely moving rodents. *J Neural Eng.* 2016;13:026030–026030. doi: 10.1088/1741-2560/13/2/026030
33. Coronel R, de Bakker JM, Wilms-Schopman FJ, Opthof T, Linnenbank AC, Belterman CN, Janse MJ. Monophasic action potentials and activation recovery intervals as measures of ventricular action potential duration: experimental evidence to resolve some controversies. *Heart Rhythm.* 2006;3:1043–1050. doi: 10.1016/j.hrthm.2006.05.027
34. Western D, Hanson B, Taggart P. Measurement bias in activation-recovery intervals from unipolar electrograms. *Am J Physiol Heart Circ Physiol.* 2015;308:H331–H338. doi: 10.1152/ajpheart.00478.2014
35. Love MI, Huber W, Anders S. Moderated estimation of fold change and dispersion for RNA-seq data with DESeq2. *Genome Biol.* 2014;15:550. doi: 10.1186/s13059-014-0550-8
36. Chen Y, Lun AT, Smyth GK. From reads to genes to pathways: differential expression analysis of RNA-Seq experiments using Rsubread and the edgeR quasi-likelihood pipeline. *F1000Res.* 2016;5:1438. doi: 10.12688/f1000research.8987.2
37. Yu G, Wang LG, Han Y, He QY. clusterProfiler: an R package for comparing biological themes among gene clusters. *OMICS.* 2012;16:284-7. doi: 10.1089/omi.2011.0118
38. Streicher JM, Ren S, Herschman H, Wang Y. MAPK-activated protein kinase-2 in cardiac hypertrophy and cyclooxygenase-2 regulation in heart. *Circ Res.* 2010;106:1434–1443. doi: 10.1161/CIRCRESAHA.109.213199
39. Landstrom AP, Dobrev D, Wehrens XHT. Calcium signaling and cardiac arrhythmias. *Circ Res.* 2017;120:1969–1993. doi: 10.1161/CIRCRESAHA.117.310083
40. Kong Q, Blanton RM. Protein kinase G I and heart failure: shifting focus from vascular unloading to direct myocardial antiremodeling effects. *Circ Heart Fail.* 2013;6:1268–1283. doi: 10.1161/CIRCHEARTFAILURE.113.000575
41. Gaborit N, Le Bouter S, Szuts V, Varro A, Escande D, Nattel S, Demolombe S. Regional and tissue specific transcript signatures of ion channel genes in

the non-diseased human heart. *J Physiol.* 2007;582(pt 2):675–693. doi: 10.1113/jphysiol.2006.126714
42. Qin D, Singh JP. Low-level tragus stimulation for atrial fibrillation: a glimpse of hope for neuromodulation? *JACC Clin Electrophysiol.* 2020;6:292–294. doi: 10.1016/j.jacep.2020.01.003
43. Stavrakis S, Stoner JA, Humphrey MB, Morris L, Filiberti A, Reynolds JC, Elkholey K, Javed I, Twidale N, Riha P, et al. TREAT AF (Transcutaneous Electrical Vagus Nerve Stimulation to Suppress Atrial Fibrillation): a randomized clinical trial. *JACC Clin Electrophysiol.* 2020;6:282–291. doi: 10.1016/j.jacep.2019.11.008
44. Stavrakis S, Humphrey MB, Scherlag BJ, Hu Y, Jackman WM, Nakagawa H, Lockwood D, Lazzara R, Po SS. Low-level transcutaneous electrical vagus nerve stimulation suppresses atrial fibrillation. *J Am Coll of Cardiol.* 2015;65:867-875.
45. Yin J, Hu H, Li X, Xue M, Cheng W, Wang Y, Xuan Y, Li X, Yang N, Shi Y, et al. Inhibition of Notch signaling pathway attenuates sympathetic hyperinnervation together with the augmentation of M2 macrophages in rats postmyocardial infarction. *Am J Physiol Cell Physiol.* 2016;310:C41–C53. doi: 10.1152/ajpcell.00163.2015
46. Hadaya J, Ardell JL. Autonomic modulation for cardiovascular disease. *Front Physiol.* 2020;11:617459. doi: 10.3389/fphys.2020.617459
47. McGuirt AS, Schmacht DC, Ardell JL. Autonomic interactions for control of atrial rate are maintained after SA nodal parasympathectomy. *Am J Physiol.* 1997;272(6 Pt 2):H2525–H2533. doi: 10.1152/ajpheart.1997.272.6.H2525
48. Coote JH. Myths and realities of the cardiac vagus. *J Physiol.* 2013;591:4073–4085. doi: 10.1113/jphysiol.2013.257758
49. Rysevaite K, Saburkina I, Pauziene N, Vaitkevicius R, Noujaim SF, Jalife J, Pauza DH. Immunohistochemical characterization of the intrinsic cardiac neural plexus in whole-mount mouse heart preparations. *Heart Rhythm.* 2011;8:731–738. doi: 10.1016/j.hrthm.2011.01.013
50. Nalliah CJ, Bell JR, Raaijmakers AJA, Waddell HM, Wells SP, Bernasochi GB, Montgomery MK, Binny S, Watts T, Joshi SB, et al. Epicardial adipose tissue accumulation confers atrial conduction abnormality. *J Am Coll Cardiol.* 2020;76:1197–1211. doi: 10.1016/j.jacc.2020.07.017
51. Allessie MA, Boyden PA, Camm AJ, Kléber AG, Lab MJ, Legato MJ, Rosen MR, Schwartz PJ, Spooner PM, Van Wagoner DR, et al. Pathophysiology and prevention of atrial fibrillation. *Circulation.* 2001;103:769–777. doi: 10.1161/01.cir.103.5.769
52. Tabereaux PB, Walcott GP, Rogers JM, Kim J, Dosdall DJ, Robertson PG, Killingsworth CR, Smith WM, Ideker RE. Activation patterns of Purkinje fibers during long-duration ventricular fibrillation in an isolated canine heart model. *Circulation.* 2007;116:1113–1119. doi: 10.1161/CIRCULATIONAHA.107.699264
53. Boukens BJ, Benjacholamas V, van Amersfoort S, Meijborg VM, Schumacher C, Jensen B, Haissaguerre M, Wilde A, Prechawat S, Huntrakul A, et al. Structurally abnormal myocardium underlies ventricular fibrillation storms in a patient diagnosed with the early repolarization pattern. *JACC Clin Electrophysiol.* 2020;6:1395–1404. doi: 10.1016/j.jacep.2020.06.027
54. Behr ER, Ben-Haim Y, Ackerman MJ, Krahn AD, Wilde AAM. Brugada syndrome and reduced right ventricular outflow tract conduction reserve: a final common pathway? *Eur Heart J.* 2021;42:1073–1081. doi: 10.1093/eurheartj/ehaa1051